Double Gaussian distribution of barrier height observed in densely packed GaN nanorods over Si (111) heterostructures

Lokesh Mohan,[1] Greeshma Chandan,[1] Shruthi Mukundan,[1] Basanta Roul,[1,2] and S. B. Krupanidhi[1,a)]
[1]*Materials Research Centre, Indian Institute of Science, Bangalore 560012, India*
[2]*Central Research Laboratory, Bharat Electronics, Bangalore 560013, India*

(Received 1 September 2014; accepted 9 December 2014; published online 19 December 2014)

GaN nanorods were grown by plasma assisted molecular beam epitaxy on intrinsic Si (111) substrates which were characterized by powder X-ray diffraction, field emission scanning electron microscopy, and photoluminescence. The current–voltage characteristics of the GaN nanorods on Si (111) heterojunction were obtained from 138 to 493 K which showed the inverted rectification behavior. The *I-V* characteristics were analyzed in terms of thermionic emission model. The temperature variation of the apparent barrier height and ideality factor along with the non-linearity of the activation energy plot indicated the presence of lateral inhomogeneities in the barrier height. The observed two temperature regimes in Richardson's plot could be well explained by assuming two separate Gaussian distribution of the barrier heights. © *2014 AIP Publishing LLC*.
[http://dx.doi.org/10.1063/1.4904749]

INTRODUCTION

GaN based devices are finding increased attention among the researchers working on high voltage, high frequency, and high power devices[1] due to their wide and direct bandgap (3.4 eV),[2] high critical field (3.5 MV/cm),[3] and high saturation electron velocity (2.5×10^7 cm/s)[3]. Also, the high absorption coefficient of GaN and tunability of band gap by addition of In or Al has led to huge potential in optoelectronic devices.[4,5] Therefore, the current transport studies across the GaN-Si heterojunction are crucial for its integration into the existing Silicon technology. Because of their high surface to volume ratio nano-wires based gas sensors and photodetectors have proved to be better than the epilayers based devices,[6] which has aroused much interest among the researchers recently[7–10] for the adaptability of nano-structures in devices. However, due to complexities involved in device fabrication and low yield of single nano-wires based devices, the devices based upon an ensemble of nanostructures are more preferred.[6,11] Recently Chenet *et al.*[12] and Osinsky *et al.*[13] have shown GaN epilayer based UV detectors using Schottky contact with Pd metal. Andres de Luna Bugallo *et al.*[14] reported p-i-n junction UV detectors based on an ensemble of GaN nano-wires. However, no direct report on UV detectors based on GaN nano-rods on Silicon substrate was found in the open literature, which served as a motivation for the present work. In this work, we have studied the transport properties across the metallurgical junction of GaN-nanorods grown hetero-epitaxially on Si (111) by plasma assisted molecular beam epitaxy (PAMBE). There exists a huge band gap difference between GaN (3.4 eV) and Silicon (1.12 eV) and a difference of almost 1 eV in electro-negativity between the two semiconductors which suggests the existence of a Schottky kind of barrier at the junction as has been reported in similar systems[15] and is well explained analytically.[16] The temperature dependent *I-V* characteristics are crucial to understand the nature of barrier formation and conduction process. In this work the observed temperature dependence of barrier height and ideality factor have been explained on the basis of barrier inhomogeneities assuming thermionic emission dominated transport.

EXPERIMENTAL PROCEDURE

GaN nanostructures were grown on un-doped Si (111) wafer of thickness 0.5 mm and resistivity $> 1000\,\Omega$ cm Supplied by MTI Corporation using PAMBE. Before growth the wafer was first chemically cleaned as described elsewhere.[17] It was then dipped in 10% HF for 1 min to remove the oxide layer from Silicon surface. The wafer was then loaded into the chamber to be again thermally cleaned at 700 °C for 30 min to ensure desorption of any residual oxide contamination on the surface. The nitridation of the surface was carried out at the same temperature (700 °C) for 30 min. A low temperature buffer layer growth of GaN at 500 °C was carried out before increasing the substrate temperature to 730 °C for a 3 h growth of GaN nanostructures. During growth, the temperature of the Gallium cell was kept at 950 °C which corresponds to a Gallium Beam Equivalent Pressure (BEP) of 5.65×10^{-7}mbar and the Nitrogen flow to the RF source was maintained at 1sccm at a power of 350 W.

The as grown samples were characterized by powder X-Ray Diffraction (XRD), Field Emission Scanning Electron Microscopy (FESEM), Transmission Electron Microscopy (TEM) and Photoluminescence (PL) before investigating the temperature dependent *I-V* behavior of the sample using a Kithely-236 source meter from 138 to 493 K. To prepare a well dispersed TEM sample, a piece of the as grown sample is sonicated in Acetone for 30 min. The substrate is then

a)Author to whom correspondence should be addressed. Electronic mail: sbk@mrc.iisc.ernet.in

taken out and the solution is drop-casted on the TEM grid using a micro pipette. The TEM grid is now placed under an IR lamp for drying for 2 h. The prepared sample is then kept in 12 h desiccation before going for the TEM. The two ohmic contacts for *I-V* measurement are formed by thermally evaporating Aluminum metal ~200 nm using a physical mask with circular holes of diameter 600 μm. The area of the junction is ~20 mm^2.

RESULTS AND DISCUSSION

The phase formation was confirmed by powder XRD which showed the peaks at 2θ values 28.44, 34.61, and 72.92° attributed to Si (111), GaN (0002), and GaN (0004) planes, respectively, which is shown in Fig. 1. The FESEM image in Fig. 2 shows the tilted view of the surface which establishes the growth of densely packed GaN Nanorods. The TEM image shown in the inset of Fig. 2 gives the length and diameter of the nanorods as ~250 nm and ~ 50 nm, respectively. The room temperature PL spectra of the sample shown in Fig. 3 were obtained using a He-Cd laser of wavelength 325 nm at 30 mW. The PL measurement revealed a near band edge emission peak at around 3.43 eV. We also observed a broad yellow luminescence which can be modeled as the result of a radiative recombination process between a shallow donor level near the conduction band edge and a deep gap state which acts either as a double donor or as an acceptor level.[18–20]

In PL data, the ratio of peak intensity of yellow luminescence to near band edge emission (I_{YL}/I_{NBE}) is approximately 0.05. However, its presence indicates the existence of defect states which may affect the conductivity of GaN nanorods. In the experiment, we are looking at the linear portion of forward characteristics of the GaN/Si heterojunction. For low applied voltages, the potential drop due to the resistance

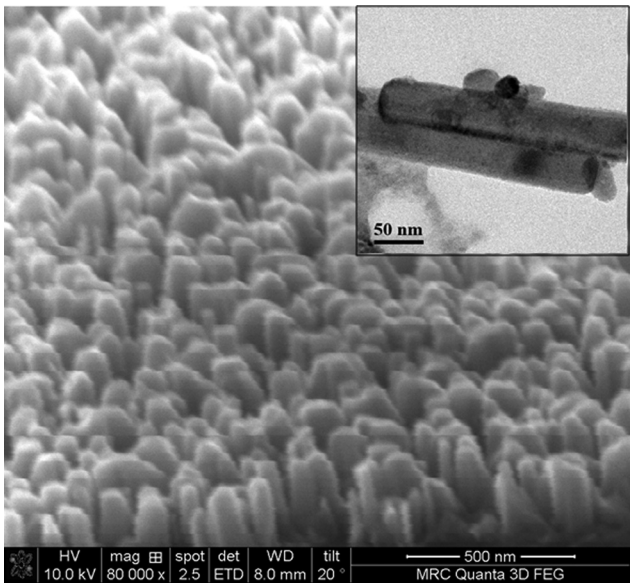

FIG. 2. FESEM image showing densely packed GaN nanorods. Inset showing TEM image of nanorods.

of the semiconductor is negligible thus ensuring that the entire potential drop is across the hetero-junction. And hence the role of a change in conductivity of GaN nanorods because of vacancy induced impurities is insignificant in *I–V* characteristics. However, the barrier height is arising as a result of the alignment of Fermi levels across the junction. In case of high electron concentration in GaN due to Nitrogen vacancies the Fermi level will shift upwards which will lead to increase in barrier height and hence a smaller current. In this regard, reducing the yellow luminescence peak in PL is important.

The temperature dependent current-voltage characteristics for the sample are shown in Fig. 4(a). The inset of

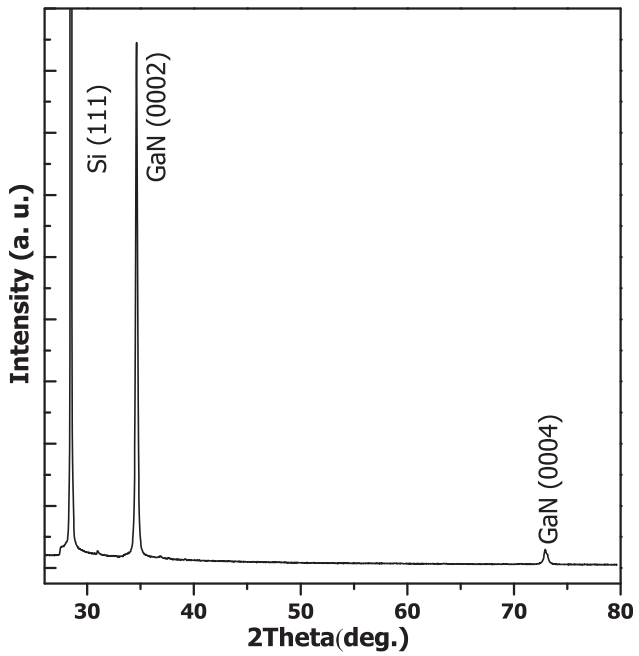

FIG. 1. Powder X-Ray diffraction showing formation of GaN (002) phase on Silicon (111) substrate.

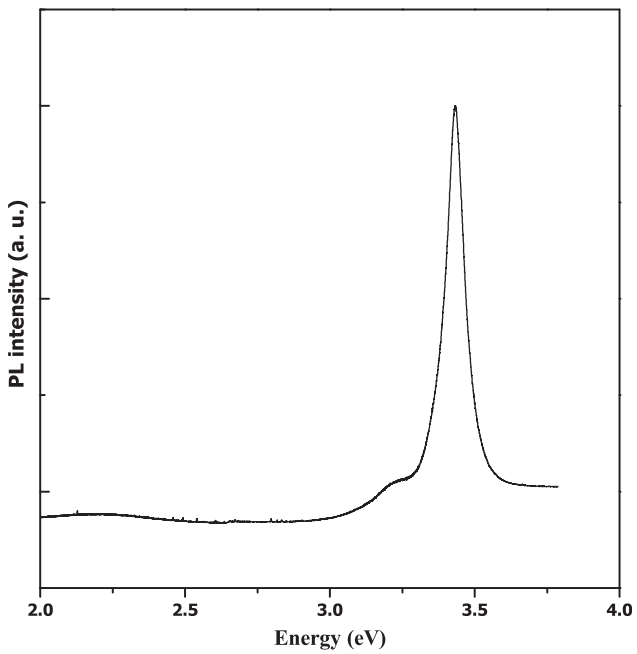

FIG. 3. Room temperature PL spectra of GaN nanorods showing near band edge emission at around 3.43 eV.

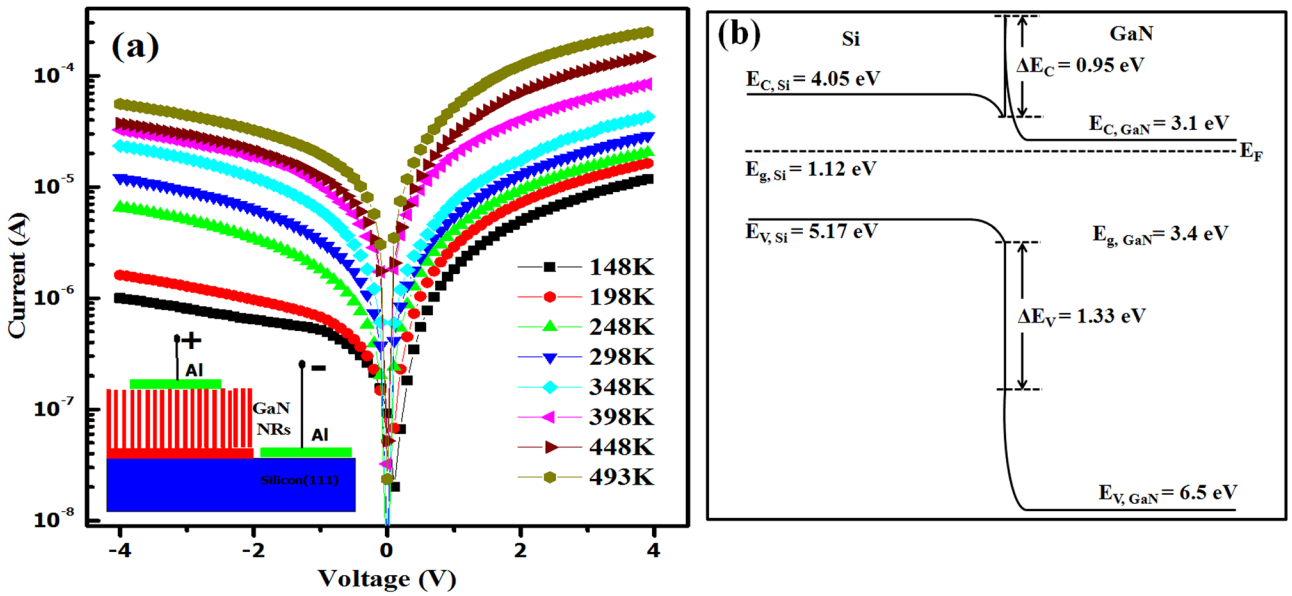

FIG. 4. (a) The temperature dependent current-voltage characteristics of GaN/Si heterojunction. The inset shows the schematic diagram of the device and (b) schematic diagram of energy band alignment of GaN/Si heterojunction.

Fig. 4(a) shows the schematic diagram of the device. Positive terminal is connected to GaN and the negative terminal is connected to Si. When Si is given negative bias through Al electrode, the equilibrium at Si-GaN junction is disturbed because of a change in potential on the Si-side of the junction. This results in electron flow from Si to GaN across the junction barrier. Aluminum metal forms ohmic contact with both silicon and Gallium nitride. Hence it does not rectify the current obtained from the junction in either positive or negative cycle. This ensures that the observed rectification is due to the junction only. We noticed the inverted rectification behavior in the junction as found in similar system[21,22] which decreases with increase in temperature. The rectifying behavior may be attributed to the band bending at the metallurgical junction of GaN and Si. The electron affinity and band gap of Si are 4.05 eV and 1.12 eV, respectively, and those of GaN are 3.1 eV and 3.4 eV, respectively.[21] Since Fermi level of GaN is higher than that of Si, during junction formation electrons flow from GaN to Si, so that the Fermi levels can be aligned. This flow of electrons gives rise to an electric field near the junction which prevents further flow of electrons hence the conduction band edge bends upward in the GaN side while a dip in the conduction band edge is registered in the Si side as shown in the band diagram (Fig. 4(b)). The band diagram also indicates that an electron when crossing from Si to GaN surmounts a lower barrier height at the junction than while moving in the opposite direction. This explains the observed inverted rectification.

This electric field facilitates the current transport of the majority carriers in the forward bias and hinders it in the reverse bias thereby introducing transport asymmetry.[23] Such a behavior suggests the possibility of a transport mechanism dominated by thermionic emission across the junction.[24–27] For further investigation, the linear portion of the forward *I-V* curve was fitted at different temperatures using the thermionic emission equation. This is valid for non-degenerate semiconductors when $qV > 3kT$ (Ref. 28) and is given by

$$J = J_s \exp\left(\frac{qV}{\eta_{app} kT}\right), \tag{1}$$

$$J_s = A^* T^2 \exp\left(\frac{-q\varphi_b}{kT}\right), \tag{2}$$

where J_s, V, η_{app}, k, A^*, T, and φ_b are saturation current density, applied bias, apparent ideality factor, Boltzmann constant, effective Richardson's constant of the emitter, absolute temperature, and apparent barrier height, respectively.

For fitting purpose, the measured device area is 20 mm^2 and A^* value is taken to be 112 Acm^{-2} K^{-2} which is in accordance with the literature values.[29,30] The values of apparent barrier height φ_b and the apparent ideality factor η_{app} were obtained from fitting. Both the ideality factor and the barrier height as tabulated in Table I are found to be temperature dependent.

While apparent barrier height is observed to be increasing with increase in temperature (0.39 eV at 148 K to

TABLE I. Temperature dependence of the apparent barrier height and ideality factor.

Temperature (K)	Barrier height (eV)	Ideality factor
148	0.39	11.48
198	0.51	10.27
248	0.63	9.31
298	0.76	8.51
348	0.88	7.32
398	0.98	5.96
448	1.11	5.39
493	1.20	4.91

1.20 eV at 493 K), the value of the ideality factor decreased from 11.48 at 148 K to 4.91 at 493 K. The temperature variation of both the parameters is found to be almost linear as shown in Fig. 5. Also the barrier height is found to be linearly dependent on ideality factor as shown in Fig. 6. Such a variation is not found in registry with any of the possible barrier lowering mechanisms such as image force lowering, interfacial oxide layer, tunneling, interface states, or generation recombination processes in the depletion layer.[30] Therefore to explain this observation, it is suggested in the literature[31,32] that a lateral distribution of barrier heights may exist at the junction. By using Ballistic electron emission microscopy Palm *et al.*[33] even showed the direct images of Schottky barrier height fluctuation in gold (Au) contact on Silicon and found it to be in agreement with a Gaussian distribution as suggested by Song *et al.*[34]

If such a lateral in homogeneity of barrier heights exists, it is possible that at lower temperatures very few electrons have sufficient energy to surmount the high barrier so that the current transport is dominated by thermionic emission across the patches of lower barrier height. As the temperature increases, more and more electrons get sufficient energy to surmount the higher barriers, which result in the increase of apparent barrier height.[35] Similar observations have been well explained in the literature assuming a Gaussian distribution of barrier height,[15,26] and were explained as the result of imperfections at the junction like non-uniform interfacial layer, surface contamination, interfacial charge and local defects such as dislocations and vacancies.[30,36] Equation (2) can be rewritten as

$$\ln\left(\frac{J_s}{T^2}\right) = \ln(A^*) - \frac{q\varphi_b}{kT}. \tag{3}$$

This equation can be used to calculate the barrier height from the saturation current density values by plotting $ln(J_s/T^2)$ versus q/kT, which is called Richardson's plot. In the Richardson's plot, we got nonlinear behavior in which two different linear regions are identified as shown in Fig. 7, which is indicative of two different barrier height distributions. In the high temperature range (348 to 493 K), the barrier height and Richardson's constant obtained are 0.09 eV and 5.47×10^{-10}A cm^{-2} K^{-2} while in the low temperature regime (148 to 298 K) their values came out to be 0.04 eV and 8.23×10^{-11}A cm^{-2} K^{-2}. These values are very less than the theoretical values which is due to the temperature dependence of the apparent barrier height arising because of the lateral inhomogeneities of the barrier height at the interface.[37–39] Let us assume a Gaussian probability distribution of barrier height given by

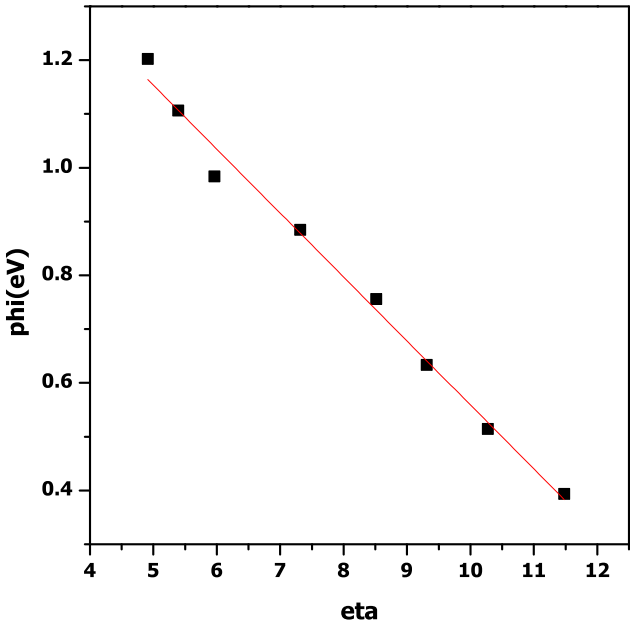

FIG. 6. Linear relationship of apparent barrier height and ideality factor.

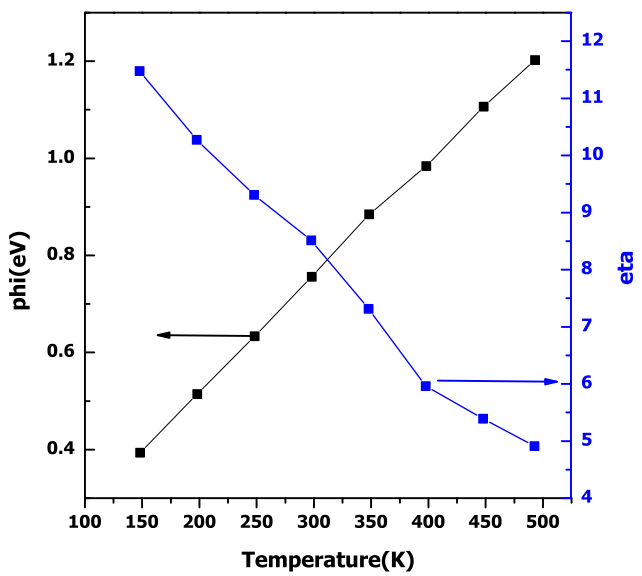

FIG. 5. Temperature dependence of apparent barrier height and ideality factor.

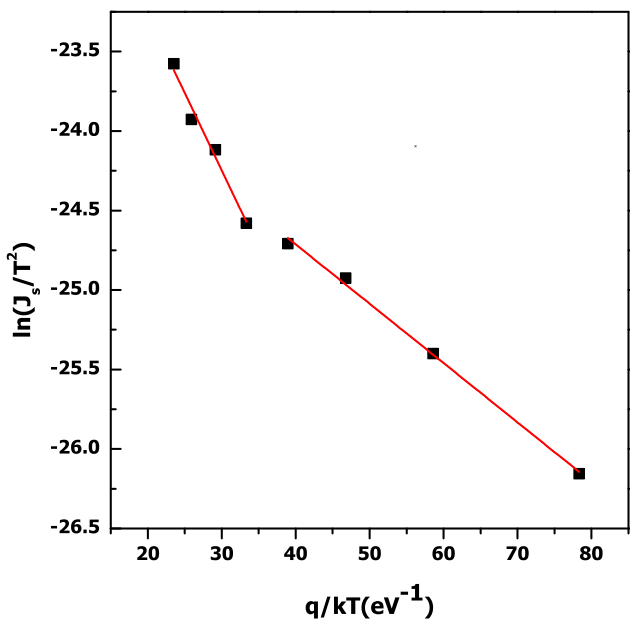

FIG. 7. Richardson's Plot $\ln(J_s/T^2)$ vs. q/kT with two identifiable linear regions.

$$P(\varphi_b) = \frac{1}{\sigma\sqrt{(2\pi)}}\exp\left(-\frac{(\varphi_b - \overline{\varphi_b})^2}{2\sigma^2}\right), \quad (4)$$

where σ is the standard deviation of the distribution function, $\overline{\varphi_b}$ is the mean value of apparent barrier height, and $1/\sqrt{(2\pi)}$ is the normallisation factor. Now the overall current across the junction will be given by

$$J = \int_{-\infty}^{\infty} J(\varphi_b, V)\, P(\varphi_b) d\varphi_b. \quad (5)$$

From thermionic emission theory, the current density across Schottky barrier is given by[40]

$$J = A^* T^2 \exp\left(-\frac{q\varphi_b}{kT}\right)\exp\left(\frac{qV}{kT}\right)\left[1 - \exp\left(-\frac{qV}{kT}\right)\right], \quad (6)$$

where all the terms have the meaning as mentioned before. On putting the values from Eqs. (4) and (6) and integrating the above expression, we get

$$J = A^* T^2 \exp\left(-\frac{q}{kT}\left(\overline{\varphi_b} - \frac{\sigma^2 q}{2kT}\right)\right)\exp\left(\frac{qV}{kT}\right) \times \left[1 - \exp\left(-\frac{qV}{kT}\right)\right]. \quad (7)$$

Let us assume the linear dependence of standard deviation and mean barrier height with applied bias

$$\sigma = \sigma_0 + \xi V, \quad (8)$$

$$\overline{\varphi_b} = \overline{\varphi_{b_0}} + \gamma V, \quad (9)$$

where ξ and γ are the coefficient of linear dependence of σ and $\overline{\varphi_b}$ on applied bias, while σ_0 and $\overline{\varphi_{b_0}}$ are zero bias standard deviation of barrier height distribution and zero bias mean barrier height respectively. Using Eq. (8) together with Eq. (9) in Eq. (7) and neglecting the $\xi^2 V^2$ term, we obtain

$$J = A^* T^2 \exp\left(-\frac{q\varphi_{ap}}{kT}\right)\exp\left(\frac{qV}{\eta_{ap} kT}\right)\left[1 - \exp\left(-\frac{qV}{kT}\right)\right], \quad (10)$$

where

$$\varphi_{ap} = \varphi_b = \left(\bar{\varphi}_{b_0} - \frac{\sigma_0^2 q}{2kT}\right), \quad (11)$$

$$\frac{1}{\eta_{ap}} = (1 - \gamma) + \frac{\sigma_0 \xi q}{kT}. \quad (12)$$

$\bar{\varphi}_{b_0}$ is zero bias mean barrier height. When $qV > 3kT$, Eq. (10) reduces to

$$J = J_s \exp\left(\frac{qV}{\eta_{ap} kT}\right), \quad (13)$$

where

$$J_s = A^* T^2 \exp\left(-\frac{q\varphi_{ap}}{kT}\right). \quad (14)$$

This is the equation used for fitting experimental data. Equation (14) can be rewritten as

$$\ln\left(\frac{J_s}{T^2}\right) - \left(\frac{\sigma_0^2 q^2}{2k^2 T^2}\right) = \ln(A^*) - \frac{q\bar{\varphi}_{b_0}}{kT}, \quad (15)$$

which is called the modified Richardson's equation.

On plotting the apparent barrier height values against q/2kT, we got two linear regions in accordance with Eq. (11) as shown in Fig. 8, in the same temperature range as we got in the conventional Richardson's plot. The values of mean apparent barrier height ($\bar{\varphi}_{b_0}$) and its variance(σ_0^2) in the temperature range 148–298 K are calculated from Eq. (11) to be 1.07 eV and 0.018 eV^2, respectively, while in the higher temperature range 348–498 K these values are found to be 1.95 eV and 0.06 eV^2, respectively. In the same above mentioned temperature ranges, we again got two separate linear regions when we plotted $[(1/\eta_{app})-1]$ vs. q/kT as shown in Fig. 9. Using the obtained values of σ_0, the values of ξ are calculated to be -0.03 and -5.6×10^{-3} in the higher and lower temperature ranges, respectively. The values of γ calculated from the intercept of $[(1/\eta_{app}) - 1]$ vs. q/kT plot for the above mentioned higher and lower temperature ranges are 0.64 and 0.86, respectively. Using the obtained values of standard deviation σ_0 from φ_{ap} vs. (q/2kT) plot, the values of $\ln\left(\frac{J_s}{T^2}\right) - \left(\frac{\sigma_0^2 q^2}{2k^2 T^2}\right)$ are obtained in the two linear regions which are then used to get modified Richardson plot, which is shown in Fig. 10. The values of mean barrier height and Richardson constant obtained from this plot are found to be (1.95 eV, 100.09A cm^{-2} K^{-2}) and (1.09 eV, 368.34 A cm^{-2} K^{-2}) in the above mentioned higher and lower temperature ranges, respectively. Having the knowledge about the distribution parameters of barrier heights in a known temperature range such as its mean value and standard deviation is very important for a device designer. The realization of two different mean barrier

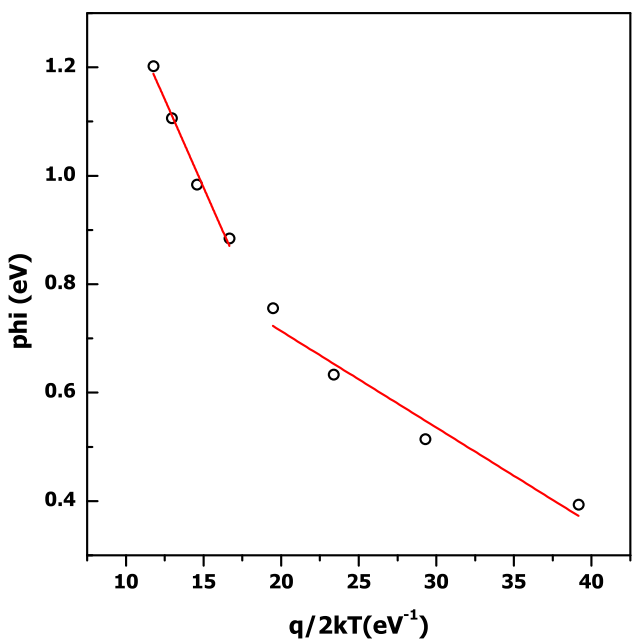

FIG. 8. Apparent barrier height vs. q/2kT plot to obtain the parameters of Gaussian distribution of barrier heights in the two linear regions.

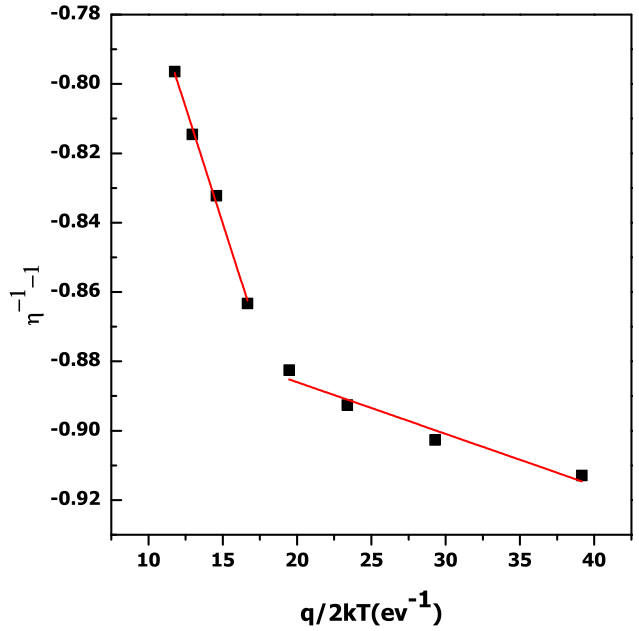

FIG. 9. $[(1/\eta_{app})-1]$ vs. q/kT gives the linear coefficient of bias dependence of apparent barrier height and its standard deviation.

heights only indicates a shift of mean barrier height value with increase in temperature. Initially not enough number of electrons has sufficient energy to cross higher barrier but as the temperature is raised more number of electrons start surmounting the higher barriers which results in the increase in the mean value of barrier height and a slight change in its variance. That is why in this particular case, we found that the observed data cannot be explained by a single Gaussian distribution function rather two different regions could well explain the observed data. The values of zero bias mean barrier height are found to be in good agreement with the values obtained from Fig. 8. The value of Richardson constant obtained from this

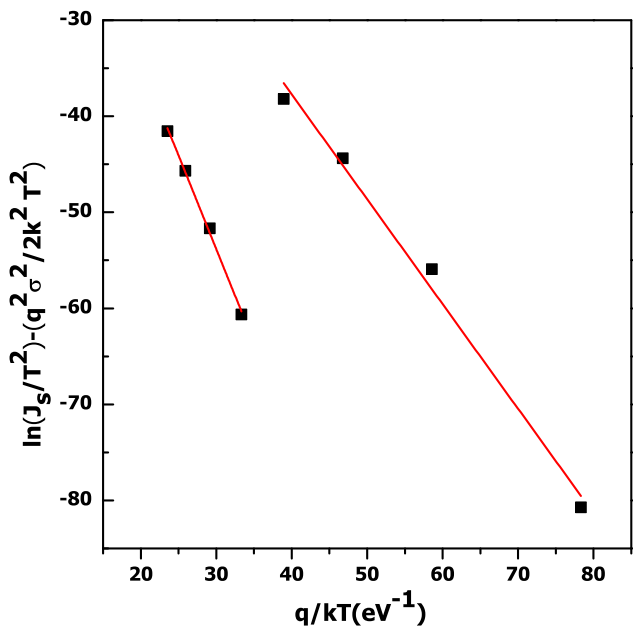

FIG. 10. Modified Richardson's plot gives zero bias mean barrier height and effective Richardson's constant in the two temperature regimes.

graph in the high temperature range is 100.09 A cm^{-2} K^{-2}, which is slightly lower than the theoretical value taken for fitting purpose. However in the low temperature range, this value is 368.34 A cm^{-2} K^{-2}. The difference of calculated A^* values may be attributed to the fluctuations in potential at the interface because of spatial variation of barrier height. [38]

CONCLUSIONS

Densely packed GaN nanorods oriented along (0002) direction are grown on Si (111) substrate by PAMBE. The formation of GaN (0002) phase is confirmed by powder XRD while FESEM images are used to see the morphology of the sample. The photoluminescence measurements showed the presence of yellow luminescence along with the near band edge emission at 3.43 eV. The TEM image shows the length of the nanorod ~250 nm and its diameter as ~50 nm.

The current-voltage characteristics of GaN on Silicon heterojunction indicated the inverted rectification character of the junction. The temperature dependence of current–voltage characteristics of the junction is explained by assuming well accepted thermionic emission model with laterally distributed barrier heights. The non-linearity of activation energy plot is explained as the result of lateral inhomogeneities of the barrier height. We found two separate linear regions in the nonlinear activation energy plot suggesting two different Gaussian distribution of barrier height in the temperature ranges (148 to 298 K) and (348 to 493 K). In 148 to 298 K, the apparent barrier height data fit well with mean barrier height 1.07 eV and variance 0.02 eV^2. The coefficients of linear dependence of mean barrier height and its standard deviation in this temperature regime are found to be 0.86 and -5.6×10^{-3}. Again in temperature range 348 to 493 K the values of mean barrier height, variance of barrier height, linear coefficient of bias dependence of mean barrier height and its variance are found to be 1.95 eV, 0.06 eV^2, 0.64, and −0.03, respectively. The values of mean barrier height and Richardson constant obtained from the modified Richardson's plot are found to be (1.95 eV, 100.09 A cm^{-2} K^{-2}) and (1.09 eV, 368.34 A cm^{-2} K^{-2}) in the above mentioned higher and lower temperature ranges, respectively.

ACKNOWLEDGMENTS

We thank Ms. Shalini Tripathi for her help in obtaining the TEM image of the GaN nanorods.

[1]U. K. Mishra, L. Shen, T. E. Kazior, and Y. F. Wu, Proc. IEEE **96**, 287 (2008).
[2]Y. Koide, H. Itoh, M. R. H. Khan, K. Hiramatu, N. Sawaki, and L. Akasak, J. Appl. Phys. **61**, 4540 (1987).
[3]T. P. Chow and R. Tyagi, IEEE Trans. Electron Devices **41**, 1481 (1994).
[4]M. Umeno, T. Egawa, and H. Ishikawa, Mater. Sci Semicond. Proc. **4**, 459 (2001).
[5]B. Zhang and Y. Liu, Chin. Sci. Bull. **59**(12), 1251 (2014).
[6]J. M. Kang, J. S. Lee, S. K. Sim, H. Kim, B. Min, K. Cho, G. T. Kim, M. Y. Sung, S. Kim, and H. S. Han, Jpn. J. Appl. Phys. **43**, 6868 (2004).
[7]T. Pauporte, O. Lupan, B. Viana, L. Chow, and M. Tchernycheva, Proc. SPIE **8987**, 89871R (2014).
[8]Y. Cui, Q. Wei, H. Park, and C. M. Lieber, Science **293**, 1289 (2001).

[9]M. Tchernycheva, P. Lavenus, H. Zhang, A. V. Babichev, G. Jacopin, M. Shahmohammadi, F. H. Julien, R. Ciechonsky, G. Vescovi, and O. Kryliouk, Nano Lett. **14**, 2456 (2014).
[10]S. Han, W. Jin, D. Zhang, T. Tang, C. Li, X. Liu, Z. Liu, B. Lei, and C. Zhou, Chem. Phys. Lett. **389**, 176 (2004).
[11]W. Guo, M. Zhang, A. Banerjee, and P. Bhattacharya, Nano Lett. **10**, 3355 (2010).
[12]Q. Chen, J. W. Yang, A. Osinsky, S. Gangopadhyay, B. Lim, M. Z. Anwar, and M. A. Khan, Appl. Phys. Lett. **70**, 2277 (1997).
[13]A. Osinsky, S. Gangopadhyay, J. W. Yang, R. Gaska, D. Kuksenkov, H. Temkin, I. K. Shmagin, Y. C. Chang, J. F. Muth, and R. M. Kolbas, Appl. Phys. Lett. **72**, 551 (1998).
[14]A. de Luna Bugallo, M. Tchernycheva, G. Jacopin, L. Rigutti, F. H. Julien, S. T. Chou, Y. T. Lin, P. H. Tseng, and L. W. Tu, Nanotechnology **21**, 315201 (2010).
[15]B. Roul, T. N. Bhat, M. Kumar, M. K. Rajpalke, N. Sinha, A. T. Kalghatgi, and S. B. Krupanidhi, Solid State Commun. **151**, 1420 (2011).
[16]M. Gil, J. Yang, and R. N. Kleiman, IEEE Trans. Electron Devices **61**, 198 (2014).
[17]M. Kumar, M. K. Rajpalke, B. Roul, T. N. Bhat, N. Sinha, A. T. Kalghatgi, and S. B. Krupanidhi, Appl. Surf. Sci. **257**, 2107 (2011).
[18]T. Suski, P. Perlin, H. Teisseyre, M. Leszczynski, I. Grzegory, J. Jun, M. Bockowski, S. Porowski, and T. D. Moustakas, Appl. Phys. Lett. **67**, 2188 (1995).
[19]D. C. Reynolds, D. C. Look, B. Jogai, J. E. V. Nostrand, R. Jones, and J. Jenny, Solid State Commun. **106**, 701 (1998).
[20]D. M. Hofmann, D. Kovalev, G. Steude, B. K. Meyer, A. Hoffmann, L. Eckey, R. Heitz, T. Detchprom, H. Amano, and I. Akasaki, Phys. Rev. B **52**, 16702 (1995).
[21]T. N. Bhat, M. K. Rajpalke, B. Roul, M. Kumar, and S. B. Krupanidhi, J. Appl. Phys. **110**, 093718 (2011).
[22]L. J. Mandalapu, F. X. Xiu, Z. Yang, and J. L. Liu, J. Appl. Phys. **102**, 023716 (2007).
[23]A. Pitanti, D. Ercolani, L. Sorba, S. Roddaro, F. Beltram, L. Nasi, G. Salviati, and A. Tredicucci, Phys. Rev. X **1**, 011006 (2011).
[24]A. K. Srivastava, J. L. Zyskind, R. M. Lum, B. V. Dutt, and J. K. Klingert, Appl. Phys. Lett. **49**, 41 (1986).
[25]E. D. Hinkley, R. H. Rediker, and D. K. Jadus, Appl. Phys. Lett. **6**, 144 (1965).
[26]S. Chand and J. Kumar, Semicond. Sci. Technol. **11**, 1203 (1996).
[27]I. Tascioglu, U. Aydemir, and S. Altındal, J. Appl. Phys. **108**, 064506 (2010).
[28]M. K. Rajpalke, T. N. Bhat, B. Roul, M. Kumar, and S. B. Krupanidhi, J. Appl. Phys. **112**, 023706 (2012).
[29]R. Sharma, J. Electron Devices **8**, 286 (2010), available at http://www.jeldev.org/8SHARMA.pdf.
[30]S. Chand and J. Kumar, J. Appl. Phys. **80**, 288 (1996).
[31]W. Monch, J. Vac. Sci. Technol. B **17**, 1867 (1999).
[32]R. F. Schmitsdorf, T. U. Kampen, and W. Monch, J. Vac. Sci. Technol. B **15**, 1221 (1997).
[33]H. Palm, M. Arbes, and M. Schulz, Phys. Rev. Lett. **71**, 2224 (1993).
[34]Y. P. Song, R. L. V. Meirhaeghe, W. H. Laflere, and F. Cardon, Solid-State Electron. **29**, 633 (1986).
[35]C. Coskun, M. Biber, and H. Efeoglu, Appl. Surf. Sci. **211**, 360 (2003).
[36]A. Hattab, J. L. Perrossier, F. Meyer, M. Barthula, H. J. Osten, and J. Griesche, Mater. Sci. Eng. B **89**, 284 (2002).
[37]J. H. Werner and H. H. Gutter, J. Appl. Phys. **69**, 1522 (1991).
[38]S. Aydogan, M. Saglam, and A. Turut, Appl. Surf. Sci. **250**, 43 (2005).
[39]C. A. Dimitriadis, S. Logothetidis, and I. Alexandrou, Appl. Phys. Lett. **66**, 502 (1995).
[40]S. M. Sze and K. K. Ng, *Physics of Semiconductor Devices* (John Wiley & Sons, New Jersey, 2007), p. 157.